A Three–Dimensional Non–Hydrostatic Model for Free Surface Flows – Development, Verification and Limitations

H. Weilbeer[1] and J. A. Jankowski[2]

Abstract

The theoretical background of a new finite–element non–hydrostatic model for simulation of free surface flows based on the fractional step method and pressure decomposition is presented. One of the verification cases concerning the solitary wave propagation is provided. Further developments concerning more sophisticated turbulence modelling for practical applications as flows around structures or scour formation are discussed and illustrated with preliminary, but very promising results.

Introduction

The standard version of the code used for simulations presented in this paper, **Telemac3D**, solves numerically the three–dimensional shallow water equations for incompressible free surface flows. The typical application domains of this model are geophysical free surface flows with complex geometry. The code was developed in Laboratoire National d'Hydraulique (Electricité de France, EDF) in Chatou by Paris, based on the experience gained with a two–dimensional code **Telemac2D** (Galland, 1991). A description of the three–dimensional, hydrostatic algorithm (**Telemac3D**) is given by Janin et al. (1997).

[1] Institute of Fluid Mechanics and Computer Applications in Civil Engineering, University of Hannover, Appelstr. 9A, D–30167 Hannover, Germany

email: weilbeer@hydromech.uni–hannover.de http://www.hydromech.uni–hannover.de

[2] Present adress:Federal Waterway Engineering and Research Institute, Kußmaulstraße 17, D–76187 Karlsruhe, Germany

email: jacek.jankowski@baw.de http://www.baw.de

Telemac3D uses the finite element method for the numerical solution. The mesh consists of a constant number of tiers of prismatic elements over the whole computational domain, so that advantage of the σ–transformation can be taken. The interpolation functions are linear, which is a good compromise between the approximation accuracy and the required computational effort. The algorithm is based on the *operator splitting* technique which yields a significantly modular algorithm structure. The code is fully vectorised using the element–by–element method and can be parallelised by domain decomposition. For solution of the linear equations appearing in various algorithm steps, iterative solvers are used.

The non–hydrostatic version of the code removes the previously existing limitations due to the hydrostatic approximation which is intrinsic in the three–dimensional shallow water equations. Two important aspects are addressed. First, the vertical acceleration in free surface incompressible flows is taken into consideration by solving the vertical momentum conservation equation. Second, the free surface computation method allows simulation of its movements without limitations typical for shallow water equations, as the restriction to long waves or to gentle slopes of the free surface and the bottom. In following the theoretical background of the non–hydrostatic model is outlined.

Non–hydrostatic model formulation

The time (t) dependend hydrodynamic equation set to be solved consists of the three–dimensional equation of motion (Navier–Stokes), the continuity equation, the transport equation for a tracer (temperature, salinity, passive effluent concentration), equation of state and an equation for the free surface position. It is formulated for geophysical free surface flows in the non–inertial, orthogonal Cartesian co–ordinate system (*x*,*y*,*z*) connected with the surface of the earth. z points vertically upward in the direction of **–g**, the acceleration of gravity. The dependend variables are velocity **u** = (*u*,*v*,*w*) and the free surface position S, as well as the pressure p. In order to simplify the basic form of the equations, a number of assumptions, approximations and simplifications is met. The flow is assumed to be incompressible, so that the density ϱ can be obtained from a separate equation of state. The variations of density $\Delta\varrho$ around an average flow density ϱ_0 are assumed to be small, so that the Boussinesq approximation is valid. The eddy viscosity (or diffusivity) concept is introduced to deal with the fluid turbulence. Leaving the description of the free surface to the next sections, the set of the governing equations can be written as follows:

$$\frac{\partial \mathbf{u}}{\partial t} + \mathbf{u}\nabla\mathbf{u} + 2\Omega \times \mathbf{u} = -\frac{1}{\rho_0}\nabla p + \frac{\rho}{\rho_0} g + \nabla \cdot (\boldsymbol{\nu}\nabla\mathbf{u}) \tag{1}$$

$$\nabla \cdot \mathbf{u} = 0 \tag{2}$$

$$\frac{\partial T}{\partial t} + \mathbf{u}\nabla T = \nabla \cdot \left(\boldsymbol{\nu}_T \nabla T\right) + q_T \tag{3}$$

$$\rho = \rho(T, s, c) \tag{4}$$

In the equation of state (4) the density is a function of transported *active tracers*, as temperature T, salinity s and/or suspended matter concentration c, but not of the pressure. The tracer transport is described using the transport equations (the equation for temperature (3) is cited above) including a source term q_T. Various turbulence models can be applied in order to obtain the values for eddy viscosity $\boldsymbol{\nu}$ and eddy diffusivity $\boldsymbol{\nu}_T$. The non–inertiality of the co–ordinate system is taken into consideration by introducing the Coriolis force term, where Ω is the angular velocity of the earth's rotation relative to the inertial system fixed to the distant stars.

For free surface tracking the *height function* method is applied. This technique is based on treating the free surface directly as a moving boundary. The distance between the interface and a given reference level is calculated from a separate equation. Therefore, it requires that the free surface can be represented by a single–value function (*height function*) S (x, y, t) with respect to one of the co–ordinate directions. This approach offers a simple and robust method of simulating environmental free surface flows. However, the restriction to single valued functions exclude some classes of flows, as e.g. breaking surfaces, bubbles, drops.

Two most widely used equations for tracking the free surface, the *kinematic boundary condition* and the *conservative free surface equation* are implemented. The first equation is obtained from kinematic conditions concerning the free surface particles:

$$\frac{\partial S}{\partial t} + u_s \frac{\partial S}{\partial x} + v_s \frac{\partial S}{\partial y} - w_s = 0 \tag{5}$$

where the suffix *s* indicates the velocity components at the free surface. The latter equation is obtained from integration of the continuity equation over the depth from the bottom z = –B(x,y) to the free surface z = S(x,y,t), using the kinematic boundary condition (5) and the impermeability condition at the bottom (similar to (5)). The obtained *conservative form of the free surface equation* is:

$$\frac{\partial S}{\partial t} + \frac{\partial}{\partial x}\int_{-B}^{S} u\,dz + \frac{\partial}{\partial y}\int_{-B}^{S} v\,dz = 0 \qquad (6)$$

Both equations mentioned above are hyperbolic. The main advantage of the conservative equation is that it includes the proper boundary conditions at the bottom and at the free surface. This approach brings a method of finding the free surface location while automatically satisfying the mass conservation criterion. However, the kinematic boundary condition allows easier implementation of some specific boundary conditions, as e.g. non–reflecting ones.

The treatment of pressure is one of the most characteristic and important features of the realised algorithm and is discussed in detail. The main idea of the new non–hydrostatic model is to decompose the pressure into two physically interpretable parts, the *hydrostatic* and *hydrodynamic* pressures, the latter treated as a form of a correction to the former. In contrast to the internal flows, in the free surface flows the pressure terms in the momentum conservation equation (1) can be separated into two terms, consisting of the *hydrostatic pressure* p_H, which can be explicitly computed, and the *hydrodynamic (motion) pressure* π, which can be found e.g. by solving a Poisson pressure equation. Therefore, in following, the global pressure p is decomposed into a sum:

$$p = p_H + \pi \qquad (7)$$

The hydrostatic pressure p_H can be computed from the free surface elevation and the local fluid density $\varrho(x,y,z)$ field by integrating the equation of hydrostatics

$$\frac{\partial p_H}{\partial z} = -\rho g \qquad (8)$$

in the water column, which yields:

$$p_H = \int_{z}^{S} \rho g\,dz = \int_{z}^{S} (\rho_0 + \Delta\rho) g\,dz = \rho_0 g(S - z) + \rho_0 g \int_{z}^{S} \frac{\Delta\rho}{\rho_0}\,dz \qquad (9)$$

As a result of this decomposition, free surface gradients independent of the density (*barotropic part*), horizontal gradients of the pressure resulting from density differences (*baroclinic part*) and gradients of the hydrodynamic pressure appear in the horizontal equations of (1) for u and v. In the vertical equation (for w) only the vertical gradient of the hydrodynamic pressure remains. Equation (1) transforms to:

$$\frac{\partial \mathbf{u}}{\partial t} + \mathbf{u}\nabla\mathbf{u} = -g\nabla_H S - g\nabla_H\left[\int_z^S \frac{\Delta\rho}{\rho_0}dz\right] - \frac{1}{\rho_0}\nabla\pi - 2\Omega \times \mathbf{u} + \nabla\cdot(\nu\nabla\mathbf{u}) \tag{10}$$

The hydrodynamic pressure π can be found from a pressure Poisson equation. Due to the algorithm structure of the model described here, a special form of this equation is applied, namely the *pressure Poisson equation from fractional step formulation*. This equation is obtained from the *time–discretised* form of the Navier–Stokes equations. In the solution algorithm the velocity time derivative is treated explicitly and can be split into:

$$\frac{\partial \mathbf{u}}{\partial t} = \frac{\mathbf{u}^{n+1} - \tilde{\mathbf{u}}}{\Delta t} + \frac{\tilde{\mathbf{u}} - \mathbf{u}^n}{\Delta t} \tag{11}$$

where $\tilde{\mathbf{u}}$ is an intermediate solution for the velocity field, which does not need to satisfy the incompressibility condition. In this way equation (10) can be transformed into an equation containing all terms but hydrodynamic pressure gradients and a second one containing them exclusively:

$$\frac{\tilde{\mathbf{u}} - \mathbf{u}^n}{\Delta t} + \mathbf{u}\nabla\mathbf{u} = -g\nabla_H S - g\nabla_H\left[\int_z^S \frac{\Delta\rho}{\rho_0}dz\right] - \frac{1}{\rho_0}\nabla\pi - 2\Omega \times \mathbf{u} + \nabla\cdot(\nu\nabla\mathbf{u}) \tag{12}$$

$$\frac{\mathbf{u}^{n+1} - \tilde{\mathbf{u}}}{\Delta t} = -\frac{1}{\rho_0}\nabla\pi \tag{13}$$

Taking into consideration that the resulting field $\mathbf{u}^{n+1}$ must fulfil the incompressible continuity equation (2), the following form of the Poisson equation for the hydrodynamic pressure can be derived from (13):

$$\nabla^2\pi = \frac{\rho_0}{\Delta t}\nabla\cdot\tilde{\mathbf{u}} \tag{14}$$

Consequently, the equation (13) can be used to find the final (and divergence–free) velocity field at the time level n+1.

The boundary conditions for the Poisson equation for the hydrodynamic pressure (14) require attention. For example, it should be realised that setting the imposed (Di-

richlet) value of zero for hydrodynamic pressure at a boundary has the physical meaning of applying purely hydrostatic pressure there. Hydrostatic pressure means no fluid motion, or that hydrostatic approximation is assumed to be valid. The hydrostatic approximation $\pi = 0$ is an acceptable boundary condition for open *inflow boundary sections*, where the velocity is thoroughly defined and its divergence is zero. For viscous flows, at the open boundaries and at free surface, the dynamic boundary conditions can be implemented:

$$\pi = \rho\nu\mathbf{u} \cdot \nabla\mathbf{u}_n \tag{15}$$

where outside pressures and stresses (e.g. wind) are neglected for simplicity and $\mathbf{n}$ represents the normal vector to the boundary. Physical reasoning yields that for those *outflow sections* where $\mathbf{n} \cdot \nabla\mathbf{u}_n = 0$, the expression $\mathbf{n} \cdot \nabla\pi = 0$ is also valid. A Neumann boundary condition for the pressure Poisson equation (14) at the *solid walls* or at the *bottom* can be obtained from the equations (13) and the impermeability condition for the final velocity $\mathbf{n} \cdot \mathbf{u}^{n+1} = 0$, which yields:

$$\mathbf{n} \cdot \nabla\pi = \frac{\rho_0}{\Delta t}\tilde{\mathbf{u}}_n \tag{16}$$

Condition (16) imposes another constraint upon the hydrodynamic pressure field to be obtained from (14). Namely, it should provide not only the final solenoidal field but also the fulfillment of the impermeability condition at the solid walls. The disadvantage of this method lies in fact that it requires a very good approximation of pressure derivatives at boundaries. However, the values of $\tilde{\mathbf{u}}_n$ are set to 0 by already applying the incompressibility boundary condition in the hydrostatic part of equation (12). In this case, the boundary condition (16) transforms to $\mathbf{n} \cdot \pi = 0$.

The solution algorithm

The algorithm applied in this model is based on the family of methods known under the common name of *decoupled methods*, where the solution of equation (1) is obtained in consecutive stages. The main idea of these methods is to solve sequentially a number of smaller, linear equation systems instead of an iterative solution of a larger, usually non–linear and slowly converging one. The free surface equation is also solved in a separate step. A number of these methods appear under various names, as *splitting schemes* (Galland (1991)), *fractional step schemes* (Quartapelle (1993)), *projection methods* (Chorin (1968), Gresho (1990), Shen (1993)) or *pressure methods* (Bulgarelli (1984), Casulli (1995)).

The solution is obtained in subsequent stages (*fractional step*) treating equations split into parts which have well–defined mathematical properties, so that the most adequate methods for a given differential operator type can be used (*operator–splitting*). In the particular case of the finite–element method, the decoupled algorithm structure allows application of equal–order linear interpolation functions for all variables. It is presumed, that the *Ladyzhenskaya–Babuska–Brezzi condition* (LBB–condition, Brezzi (1991)) is circumvented by the fact that the decoupled methods do not require an incompressibility condition in the form of an explicit equation $\nabla \cdot \mathbf{u} = 0$ occurring in the global equation set. The incompressibility is asymptotically achieved by the convergence of a pressure equation solution.

The time derivatives of the variables are split into fractional steps with respect to the mathematical operator properties and treated with appropriate numerical methods:

$$\frac{\partial \mathbf{u}}{\partial t} = \frac{\mathbf{u}^{n+1} - \mathbf{u}^{\mathbf{d}}}{\Delta t} + \frac{\mathbf{u}^{\mathbf{d}} - \mathbf{u}^{a}}{\Delta t} + \frac{\mathbf{u}^{\mathbf{a}} - \mathbf{u}^{n}}{\Delta t} \tag{17}$$

In the first step of the non–hydrostatic algorithm the hydrodynamic pressure is excluded and only the hydrostatic pressure part is taken into consideration. In this stage (advection–diffusion), the intermediate solution for the velocity field $\mathbf{u}^{d} = \tilde{\mathbf{u}}$ is obtained:

$$\frac{\mathbf{u}^{d} - \mathbf{u}^{n}}{\Delta t} + \mathbf{u}\nabla\mathbf{u} = \nabla \cdot (\nu\nabla\mathbf{u}) + \mathbf{F}_{u} \tag{18}$$

where the source terms $\mathbf{F}_{\mathbf{u}}$ are:

$$\mathbf{F}_{u} = -g\nabla_{H}S^{n} - g\nabla_{H}\left[\int_{z}^{S^{n}} \frac{\Delta\rho^{n}}{\rho_{0}} dz\right] - 2\Omega \times \mathbf{u}^{n} + \mathbf{q}_{\mathbf{u}} \tag{19}$$

According to the operator–splitting scheme, this stage is realised in two substeps, advection (hyperbolic) step and diffusion (parabolic) step, when the method of characteristics for advection, and semi–implicit standard Galerkin FEM for diffusion is required:

$$\frac{\mathbf{u}^{a} - \mathbf{u}^{n}}{\Delta t} + \mathbf{u} \cdot \nabla\mathbf{u} = 0 \tag{20}$$

$$\frac{\mathbf{u}^{d} - \mathbf{u}^{a}}{\Delta t} = \nabla \cdot (\boldsymbol{\nu}\nabla\mathbf{u}) + \mathbf{F}_{\mathbf{u}} \tag{21}$$

When the semi–implicit streamline upwind Petrov–Galerkin (SUPG) FEM for advection is chosen, the advection and diffusion steps are realised simultaneously. In general, the intermediate velocity field $\mathbf{u^d}$ is not solenoidal and its divergence is non–zero. Its value yields the source term for the (elliptic) Poisson equation for the hydrodynamic pressure (14), which is solved in the next algorithm stage (*continuity stage*) using standard Galerkin FEM with appropriate boundary conditions.

Consequently, the intermediate solution yielded by the advection–diffusion steps is corrected by the non–hydrostatic component. This component is computed from the hydrodynamic pressure gradients (equation (13)) under the assumption that the resulting final velocity must be divergence–free in the entire domain (incompressible flow) and satisfies appropriate boundary conditions:

$$\mathbf{u}^{n+1} = \mathbf{u}_d - \frac{\Delta t}{\rho_0}\nabla\pi \tag{22}$$

In this step the formal *velocity projection* (to the space of divergence–free vectors) is performed.

Finally, the free surface is found solving alternatively (5) or (6), which are hyperbolic equations solved with the method of characteristics or the semi–implicit SUPG FEM. The position of the advancing surface is tracked using a Lagrangian approach, where the mesh is adapted to the position of the free surface at each time step (so–called σ–mesh).

Model verification

Verification of the algorithm has been performed using a number of benchmark test cases covering the targeted model application domain. They include free surface and internal waves, sub– and supercritical channel flow over a steep ramp, wind– and buoyancy–driven currents (Jankowski (1998)). One of the most simple, but impressive test cases is solitary wave propagation in a long channel. The solitary wave, being a non–linear wave of finite amplitude, cannot be described properly in the framework of the shallow water equations. A solitary wave is a single elevation of water surface above an undisturbed surrounding, which is neither preceded nor followed by any free surface disturbances. Neglecting dissipation, as well as bottom and lateral boundary shear, a solitary wave travels over a horizontal bottom without changing its shape and velocity. The accuracy of the model can be evaluated by comparing the amplitude and celerity of the wave with its theoretical values, as well as by observing the conservation of the wave profile as it travels.

There are numerous analytical studies of this form of non–linear finite–amplitude wave. The first approximation provided by Laitone (1960) is the most frequently used for comparative studies. For a vertical section of an infinitely long channel of an undisturbed depth h (z=0 at the undisturbed surface), the following approximate formulae for velocity components u, w, free surface elevation η, pressure p and wave celerity c of a solitary wave with a height of H are valid:

$$u = \sqrt{gh}\frac{H}{h}\operatorname{sech}^2\left[\sqrt{\frac{3}{4}\frac{H}{h^3}(x - ct)}\right] \tag{23}$$

$$w = \sqrt{3gh}\left(\frac{H}{h}\right)^{\frac{3}{2}}\left(\frac{z}{h}\right)\operatorname{sech}^2\left[\sqrt{\frac{3}{4}\frac{H}{h^3}(x - ct)}\right]\tanh\left[\sqrt{\frac{3}{4}\frac{H}{h^3}(x - ct)}\right] \tag{24}$$

$$\eta = h + H\operatorname{sech}^2\left[\sqrt{\frac{3}{4}\frac{H}{h^3}(x - ct)}\right] \tag{25}$$

$$p = \rho g(\eta - z) \tag{26}$$

$$c = \sqrt{g(H + h)} \tag{27}$$

Following the test cases provided by Ramaswamy (1990), a solitary wave described by the formulae (23)–(27) is applied in a long channel as an initial condition, and the behaviour of the solution is observed thereafter. The simulation is performed in a finite domain, so that care must be taken choosing the initial position of the wave crest in the channel. The effective wave length λ concept is applied. λ is equal to twice the length between the wave crest and a point where the free surface elevation is η(x)=0.01H. According to Laitone:

$$\lambda = 6.9\sqrt{\frac{h^3}{H}} \tag{28}$$

A long channel 600m long and 6m wide, with a constant depth of h=10 m is taken. The mesh is 6 elements wide and 600 long, with a resolution in the direction parallel to the channel axis of 1 m. It consists of 4210 nodes and 7206 elements. The three–dimensional mesh has 11 equidistantly distributed levels. Inviscid flow without shear on the walls and bottom is assumed. All boundaries are impermeable. As the initial condition the hydrostatic approximation given by formulae (23)–(27) is applied,

with a wave height of H=2m (H=0.2h) and the initial crest position is $\lambda/2 = 80$m away from the channel end, according to (28). The time step is taken as constant, $\Delta t=0.1$s, and the simulation time 40s (Courant number in the direction of wave propagation from 0.2 to about 1.0 at the wave crest).

For computation of the free surface elevation in the non–hydrostatic case the semi–implicit (Crank–Nicholson coefficient $\theta=0.55$) or implicit SUPG methods based on the kinematic boundary condition or the conservative free surface equation are applied. The hydrodynamic pressure is set to zero at the free surface and free Neumann BCs at all other boundaries are imposed.

A comparison between the hydrostatic and the non–hydrostatic solution is provided in figure 1. In contrast to the non–hydrostatic model, the hydrostatic one does not conserve the shape and amplitude of the solitary wave as it travels.

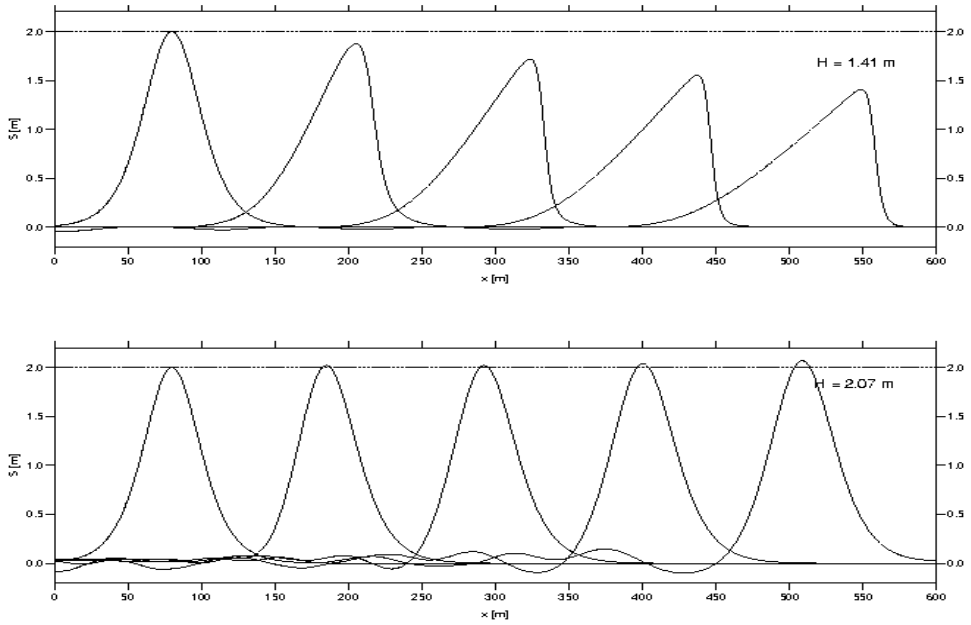

Figure 1: Solitary wave propagation in a long channel with a flat bottom. Above: hydrostatic solution. Below: non–hydrostatic solution found using free surface computation method based on the kinematic BC solved with implicit SUPG. The free surface profiles shown for t=0s, 10s, 20s, 30s, and 40s.

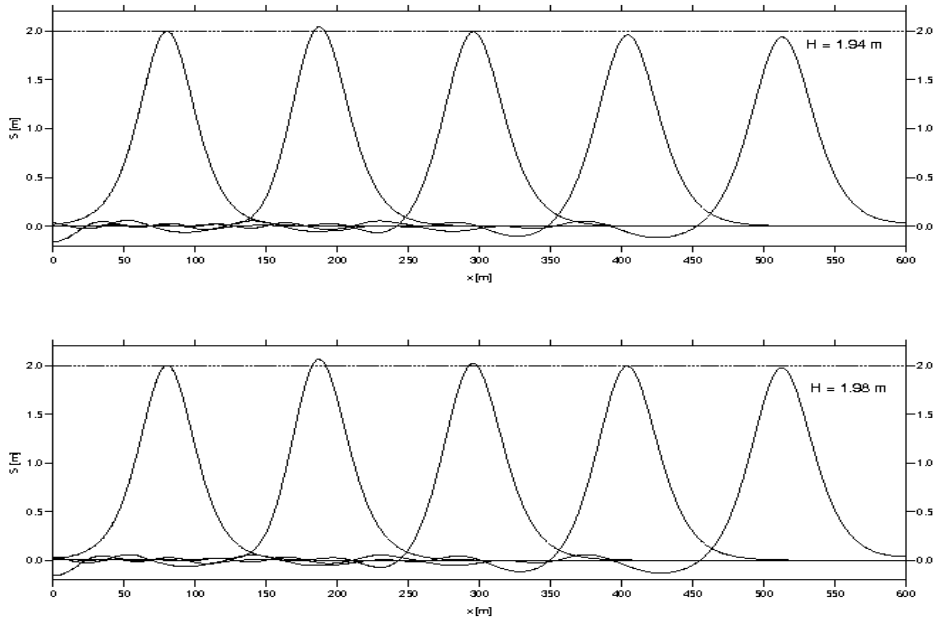

Figure 2: Solitary wave propagation in a long channel with a flat bottom for free surface computation method based on conservative free surface equation solved with SUPG. Above: implicit, below: semi–implicit θ=0.55. The free surface profiles shown for t=0s, 10s, 20s, 30s, and 40s.

The free surface schemes based on the kinematic BC show dispersive properties with ever–growing oscillations of the free surface behind the wave, while the conservative free surface algorithm is not sensitive to such effects. They are also much more sensitive to the influence of implicitness factor θ than the free surface conservative equation (Figure 2).

There are only a few restrictions limiting the application domain of the non–hydrostatic free surface model presented in this paper. Due to the σ–mesh structure, where the mesh nodes must be situated exactly along a vertical line, not all arbitrarily choosen three–dimensional geometries can be reproduced. Because of the limitations of the height function method, which requires that the free surface must be described by a single–valued function, breaking waves cannot be simulated.

Nevertheless, the ability to model three–dimensional hydrodynamical processes in the vicinity of structures is achieved for several geometries. But, in contrast to the simulations used for verification of the non–hydrostatic code which were carried out with simplest turbulence models, this aspect attracts more attention here. The second part of this paper sketches the preliminary considerations and first experience concerning the more sophisticated turbulence modeling.

Hydrodynamics in the vicinity of structures

Hydrodynamical processes in the vicinity of structures must be investigated with larger care for details. In technically relevant problems, such flows are always three–dimensional and indicate spatially strongly varying coherent turbulent structures. The horizontal and vertical scales of these flows may be of the same order of magnitude. Due to the large vertical velocities and accelerations hydrodynamical models based on the hydrostatic assumption cannot be applied.

The horseshoe vortex at the toe of a body which is induced by the stagnation pressure at the front, and the coherent turbulent structures (flow separation, periodic vortex shedding) at its rear belong to the most important and most interesting physical phenomena of flows around structures (i.e. vertical piles and abutments). They are also of practical interest. Typical technical problems directly connected with these flows are e.g. the flow and/or wave induced dynamic load of a structure or vibrations induced by oscillating loads or alternate separation processes (fluid–structure interaction). Furthermore the scour processes induced by these flows in the vicinity of structures are of vital importance in civil engineering.

Turbulence Modeling

The modeling of these phenomena is demanding for the hydrodynamical–numerical model, in particular turbulence modeling. Two totally different approaches are possible. On one hand statistical turbulence models based on the Reynolds averaged Navier–Stokes equations (RANS) are popular; on the other, large eddy simulations (LES) based on spatial filtered Navier–Stokes equations have aroused growing interest lately.

Statistical turbulence models are often applied for this task, but they are not suitable because they yield both the periodic and the turbulent fluctuations and therefore overpredict the turbulent stresses. In the case of LES the turbulent effects, which are reproducible by a given mesh resolution, are directly simulated. Only the subgrid scale turbulent stresses are taken into consideration by a turbulence model. LES concept is very promising, but seems to be too expensive for technically relevant Reynold numbers. Recently Very Large Eddy Simulations (VLES) are under development (Speziale (1998)) which can possibly close the gap between RANS and LES.

In order to gather more experience in modeling turbulent phenomena in the vicinity of structures flow around a circular cylinder is simulated, because of the broad availability of the results from experimental (e.g. Sumer (1997)) and numerical investigations (e.g. Fröhlich (1998), Breuer (1998)) for comparisons.

Examples

As mentioned above in the standard version of **Telemac3D** the turbulent viscosities can be set to constant values, or obtained from a mixing length model or a k–ε turbulence model. In the first test case an experiment was simulated which was carried out in a large wave flume. A solitary wave with a wave height of H=0,80m passes a vertical pile (diameter d=0.70m) (Figure 3). This is one of the most straightforward cases from numerous experimental series, whereby the forces induced by breaking and non–breaking waves on the vertical pile were measured. In the model, in a first attempt constant eddy viscosities for horizontal momentum exchange were chosen, and a mixing length model for vertical viscosities. As a result two symmetrical recirculation zones occur in the rear of the cylinder, but neither flow separation nor horseshoe vortex (Sumer (1997)) were observed. The forces from the solitary wave on the pile are not yet calculated.

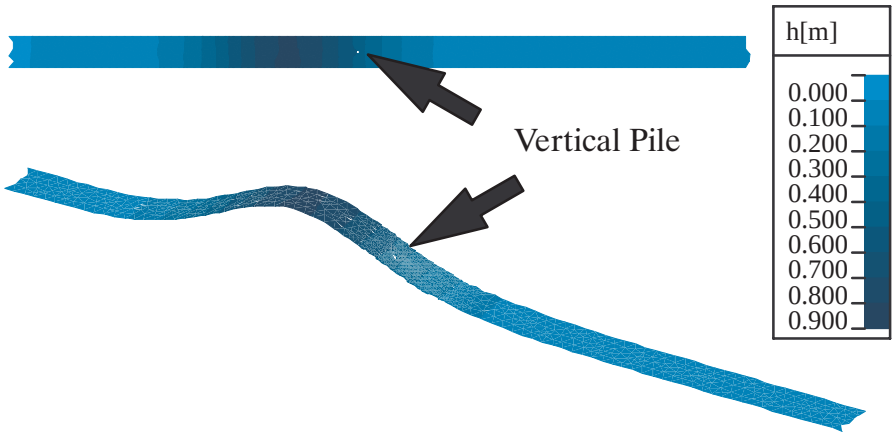

Figure 3: Solitary wave in the Large Wave Flume in Hannover.

In an next step two–dimensional simulations of a circular cylinder (d=0.10m) in a stationary flow field were carried out with **Telemac2D** in order to test different components of LES. The mesh resolution is refined nearby the walls, and no–slip boundary conditions for the velocities at the cylinder are prescribed. A two–dimensional version of the Smagorinski turbulence model is applied. It seems that the two–dimensional simulations gives a good representation of the quasi–two–dimensional mechanisms of the flow separation and the periodic vortex shedding motion (Bouris (1999), Sun (1996)). The Strouhal number of this period is in a good agreement with experimental data (St=0.21), as well as the Strouhal number of a square cylinder (St=0.14), for exact the same modelling conditions. The occurrence of a vortex street depends strongly on the grid resolution (Figure 4).

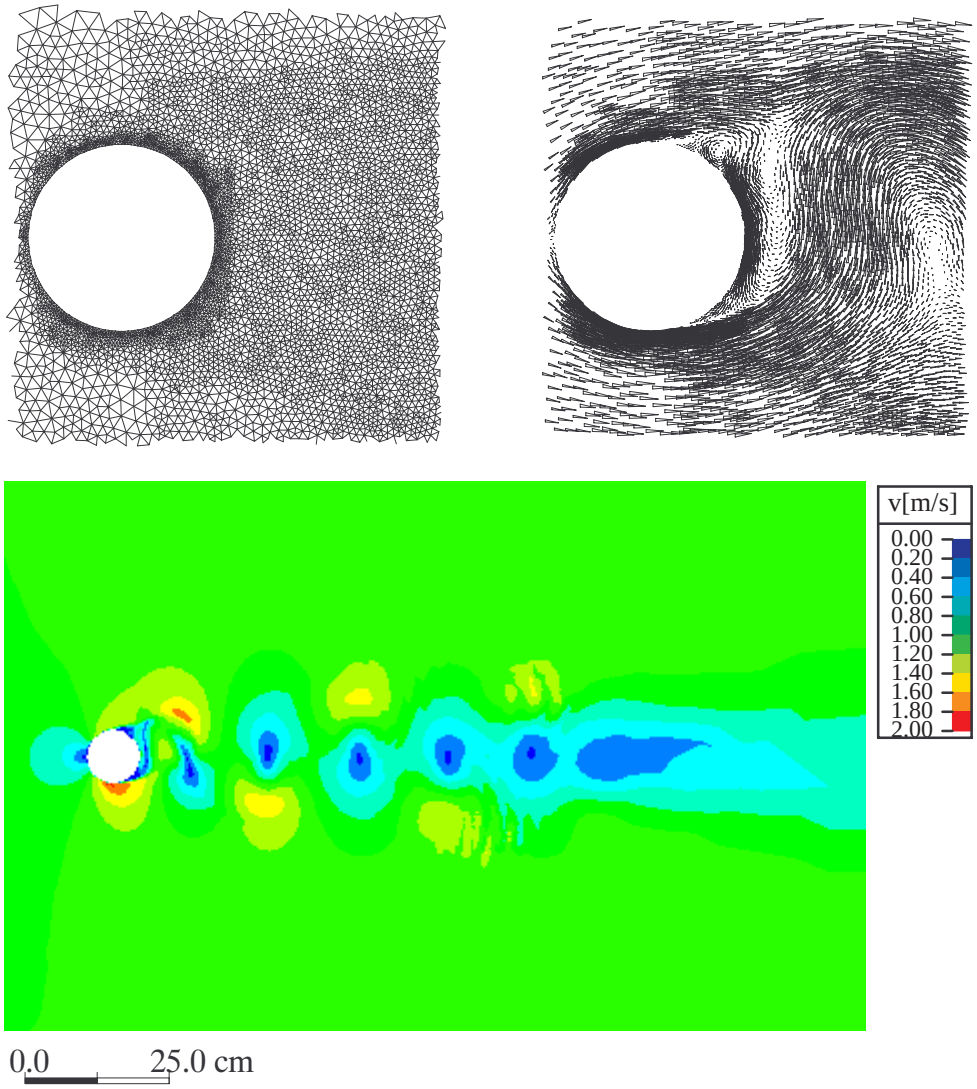

Figure 4: Zoom of the computational mesh and resulting flow velocities of a two–dimensional flow around a circular cylinder (Re=100.000, St=0.21).

The last example is included in order to illustrate the direction of future developments (Figure 5). In the same model setting as described above the flow field is calculated with the three–dimensional hydrostatic code. Sediment transport is calculated as well. A horseshoe vortex occurs which is responsible for the scour pattern in the front of the cylinder. However, by first application tests using the non–hydrostatic version, the horseshoe vortex disappears, probably due to incompatible boundary conditions. The future developments regarding three–dimensional turbulence modeling will hopefully improve the results, so it will be possible to simulate flow and sediment transport in the vicinity of structures under nonstationary conditions.

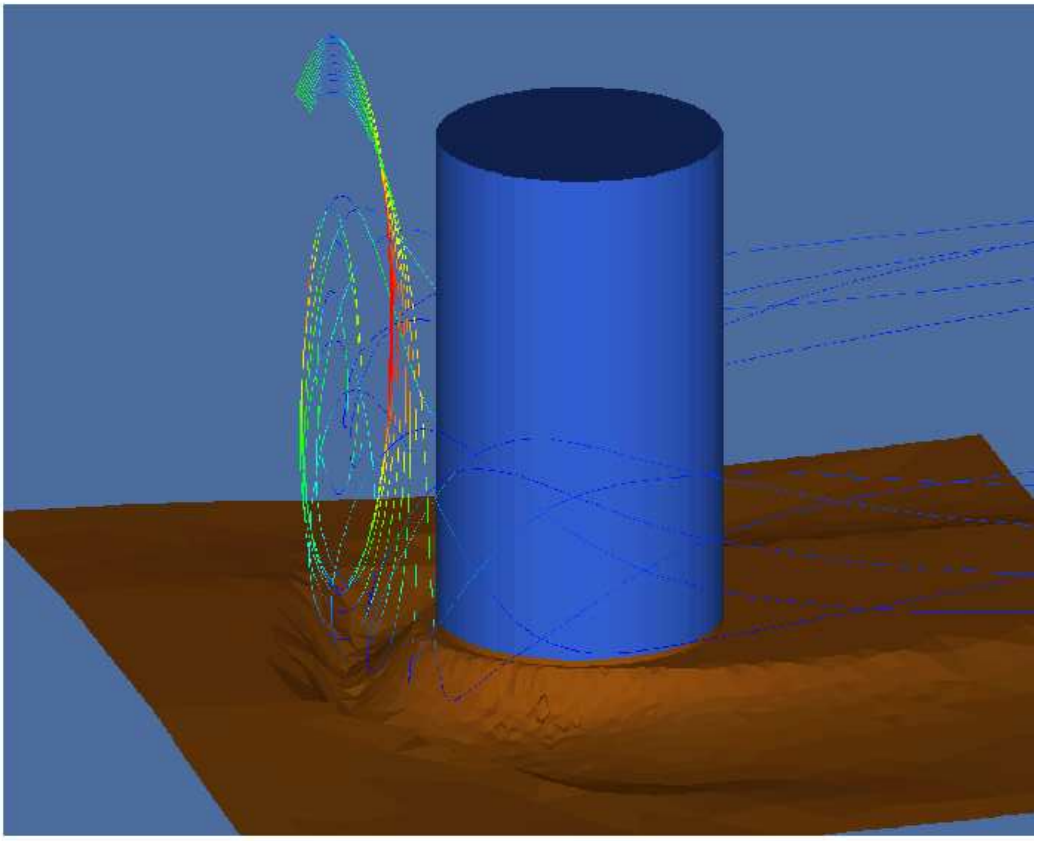

Figure 5: Horseshoe vortex in front of a circular cylinder and calculated scour pattern. The flow field and the related sediment transport is calculated using the standard code of **Telemac3D**.

Conclusions

The model presented in the paper has been developed for dealing with free surface flows, where the hydrostatic approximation is not appropriate. Only a few less important restrictions concerning the free surface shape and the boundary geometry remain. The model has been thoroughly verified using typical examples from its aimed application domain. The further developments are concentrated on more sophisticated turbulence modelling, with the accent on large eddy simulation (LES). Introductory tests using the two–dimensional model version show that this approach yields promising results. However, turbulence is a three–dimensional phenomenon, so that the fully three–dimensional approach is required.

References

[1] Bouris, D., Bergeles, G., 1999. 2D LES of vortex shedding from a square cylinder. *J. Wind Eng. Ind. Aerodyn.*, Vol. 80, 31–46.

[2] Breuer, M., 1998. Large eddy simulation of the subcritical flow past a circular cylinder: Numerical and modeling aspects. *Int. J. for Numerical Methods in Fluids*, Vol. 28, 1281–1302.

[3] Brezzi, F., Fortin, M., 1991. Mixed and hybrid finite element methods. Springer–Verlag, Berlin.

[4] Bulgarelli, U., Casulli, V., Greenspan, D., 1984. Pressure methods for the numerical solution of free surface fluid flows. Pineridge Press, Swansea, U.K.

[5] Casulli, V., Stelling, G.S., 1995. Simulation of Three–Dimensional, Non–Hydrostatic Free–Surface Flows for Estuaries and Coastal Seas. Estuarine and Coastal Modeling, Proceedings of the 4th International Conference, 1–12.

[6] Chorin, A., 1968. Numerical solution of the Navier–Stokes equations. *Math. Comp.*, 22, 745–762.

[7] Fröhlich, J., Rodi, W., Kessler, Ph., Parpais, S., Bertoglio, J.P. und Laurence, D., 1998. Large Eddy Simulation of Flow around Circular Cylinders on Structured and Unstructured Grids, in E.H. Hirschel (ed.): Notes on Numerical Fluid Mechanics, Vieweg–Verlag.

[8] Galland, J.–C., Goutal, N., Hervouet, J.–M., 1991. TELEMAC: A new numerical model for solving shallow water equations. *Adv. Water Resources*, 14 (3), 138–148.

[9] Gresho, P., 1990. On the theory of semi–implicit projection methods for viskous incompressible flows and its implementation via finite element method that also introduces a nearly consistent mass matrix. Part 1: Theory. *International Journal for Numerical Methods in Fluids*, 11, 587–620.

[10] Janin, J.–M., Marcos, F., Denot, T., 1997. Code TELEMAC–3D–Version 2.2. Note théorique. Tech. Rep. HE–42/97/049/B, Electricité de France (EDF–DER), Laboratoire National d'Hydraulique.

[11] Jankowski, J.A., 1998. A non–hydrostatic model for free surface flows. Dissertation, Institut für Strömungsmechanik und Elektronisches Rechnen im Bauwesen, Universität Hannover.

[12] Laitone, E., 1960. The second approximation to cnoidal and solitary waves. *Journal of Fluid Mechanics*, 9, 430–444.

[13] Quartapelle, L., 1993. Numerical solution of the incompressible Navier–Stokes equations. Birkhäuser, Berlin.

[14] Ramaswamy, B., 1990. Numerical simulation of unsteady viscous free surface flow. *Journal of Computational Physics*, 90, 396–430.

[15] Shen, J., 1993. A remark on the projection–3 method. *International Fournal for Numerical Methods in Fluids*, 16, 249–253.

[16] Speziale, C. G., 1998. Turbulence Modeling for Time–Depending RANS and VLES: A Review. *AIAA Journal*, Vol. 36, No.2.

[17] Sumer, B.M., Christiansen, N., Fredsøe, J., 1997. The horseshoe vortex and vortex shedding around a vertical wall–mounted cylinder exposed to waves. *J. Fluid Mechanics*, Vol. 332, 41–70.

[18] Sun, X., Dalton, C., 1996. Application of the LES method to the oscillating flow past a circular cylinder. *Journal of Fluids and Structures*, Vol. 10, 851–872.